A DYNAMICAL MODEL FOR RECEPTOR-MEDIATED CELL ADHESION TO SURFACES

DANIEL A. HAMMER AND DOUGLAS A. LAUFFENBURGER
Department of Chemical Engineering, University of Pennsylvania, Philadelphia, Pennsylvania 19104

ABSTRACT We present a dynamical model for receptor-mediated adhesion of cells in a shear field of viscous fluid to surfaces coated with ligand molecules complementary to receptors in the cell membrane. We refer to this model as the "point attachment model" because it considers the contact area between the cell and the surface to be a small, homogeneous region that mediates the initial attachment of the cell to the surface. Using a phase plane analysis of a system of nonlinear ordinary differential equations which govern the changes in free receptor density and bond density within the contact area with time, we can predict the conditions for which adhesion between the cell and the surface will take place. Whether adhesion occurs depends on values of dimensionless quantities that characterize the interaction of the cell and its receptors with the surface and its ligand, such as the bond formation rate, the receptor–ligand affinity, the fluid mechanical force, the receptor mobility, and the contact area. A key result is that there are two regimes in which different chemical and physical forces dominate: a rate-controlled high affinity regime and an affinity-controlled low-affinity regime. Many experimental observations can be explained by understanding which of these regimes is appropriate. We also provide simple approximate analytical solutions, relating adhesiveness to cell and surface properties as well as fluid forces, which allow convenient testing of model predictions by experiment.

INTRODUCTION

Cell adhesion under conditions of flow is a phenomenon of considerable importance. For example, the adhesion of blood-borne cells to the vascular surface occurs in the inflammatory response (1), cancer cell metastasis (2), and the homing of lymphocytes to Peyer's patches and lymph nodes (3, 4). Interest in cell adhesion in vivo has led to many in vitro experiments, such as the parallel plate flow chamber assay (5–7), designed to understand the physical and chemical processes that control adhesion. Also, the knowledge that subpopulations of cells have unique surface compositions has led to the development of cell separation techniques, like cell affinity chromatography (8–13), which rely on the differential adhesiveness of these subpopulations to prepared substrates. Thus, a fundamental, quantitative understanding of the adhesion of cells to surfaces can lead to understanding of in vivo phenomena, interpretation of in vitro assays, and analysis and design of biotechnological processes, which involve cell adhesion.

We focus here on the adhesion of cells to a surface when the adhesion is mediated by specific binding between molecules on the cell surface and complementary ligand molecules on the receiving surface. We build on a theoretical framework for understanding receptor-mediated cell adhesion due to Bell (14, 15). We assume the reactions of binding and dissociation occur according to characteristic rate constants, and the rates determine how many bonds form between the two surfaces during the period of close apposition. Also, we assume receptors diffuse and convect into the area of contact where binding can occur, and the rapidity of this accumulation and the size of the contact area affect the number of bonds that form. Whether the number of bonds between the cell and surface is sufficient to cause the arrest of the cell depends on the magnitude of the distractive forces, and how quickly bonds might break in response to these forces.

The model we present in this paper, which we term the "point attachment model," attempts to elucidate the dependence of adhesion on various quantities such as receptor number, binding affinity between receptor and ligand, bond formation rate, receptor diffusivity, distractive fluid forces, and contact area. We restrict our attention to cell adhesion in shear flow which is characterized by negligible inertia, and in which the cell density is low. Analysis of this system serves as a starting point for the analysis of systems inherently more complicated, like blood-borne cell–endothelial cell interactions in the vasculature.

Our emphasis in presenting this work is to predict how adhesiveness will depend quantitatively on external factors, such as changes in shear rates or temperature and to propose experiments that can serve as a direct test of those predictions. We also wish to point out significant qualitative and quantitative trends in adhesiveness that could not be predicted through intuition. Where possible, we will provide simple analytical expressions that will serve to help biological scientists interpret and predict the outcome of adhesion experiments.

D. A. Hammer's present address is School of Chemical Engineering, Cornell University, Ithaca, NY 14853.

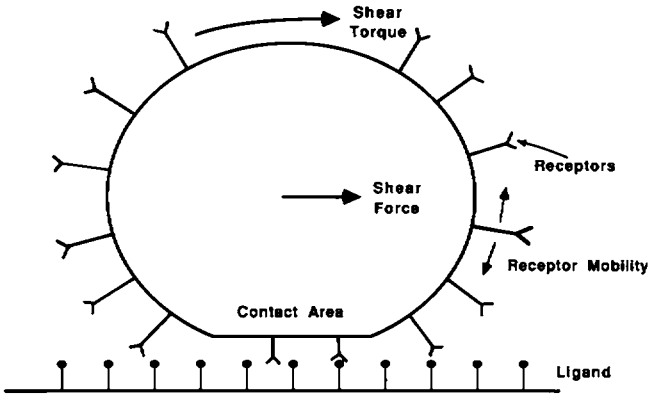

FIGURE 1 Quantities expected to influence the receptor-mediated cell adhesion to a surface include receptor number, the density of complementary surface ligands, the force and torque transmitted to the cell by the passing fluid, the mobility of receptors in the plane of the membrane, and the contact area in which cell to surface bonds may form.

MATHEMATICAL MODEL

A model intending to describe receptor-mediated cell adhesion must consider several important quantities indicated in Fig. 1. We assume the cell possesses one receptor class of number R_T available for binding. The ligand density on the substrate is N_{l_0}. Bond formation and dissociation occur according to characteristic rate constants k_f and k_r, respectively. The contact area is assumed to be a disk of radius a. Receptors have an intrinsic diffusional mobility in the plane of the membrane, D.

Our several assumptions are pictorally represented in Fig. 2. At close approach, like that needed for protein–protein molecular contact (100–300 Å), substantial pressure builds up between the cell and the surface and the portion of the cell closest to the surface flattens (16–18). The size of the flattened region depends on all the external forces and cell mechanical properties. It is this area that becomes the contact area upon molecular overlap at a separation of S_c (see Fig. 2). Given this, we assume that the contact area is well formed before molecular contact occurs. Because we are concerned with a very short time after molecular contact occurs, we assume this area remains constant throughout the analysis.

Our second critical assumption is that there is a short time, called the contact time, T_c, during which bonds can form between the cell and the surface unstressed. This is a simplification as pointed out in Fig. 2, where we schematically plot the stress seen by the bonds as a function of time along with our idealized approximation. A small stress is seen by even the first bond, but the largest stress on the bonds is due to the normal stres in the contact area that

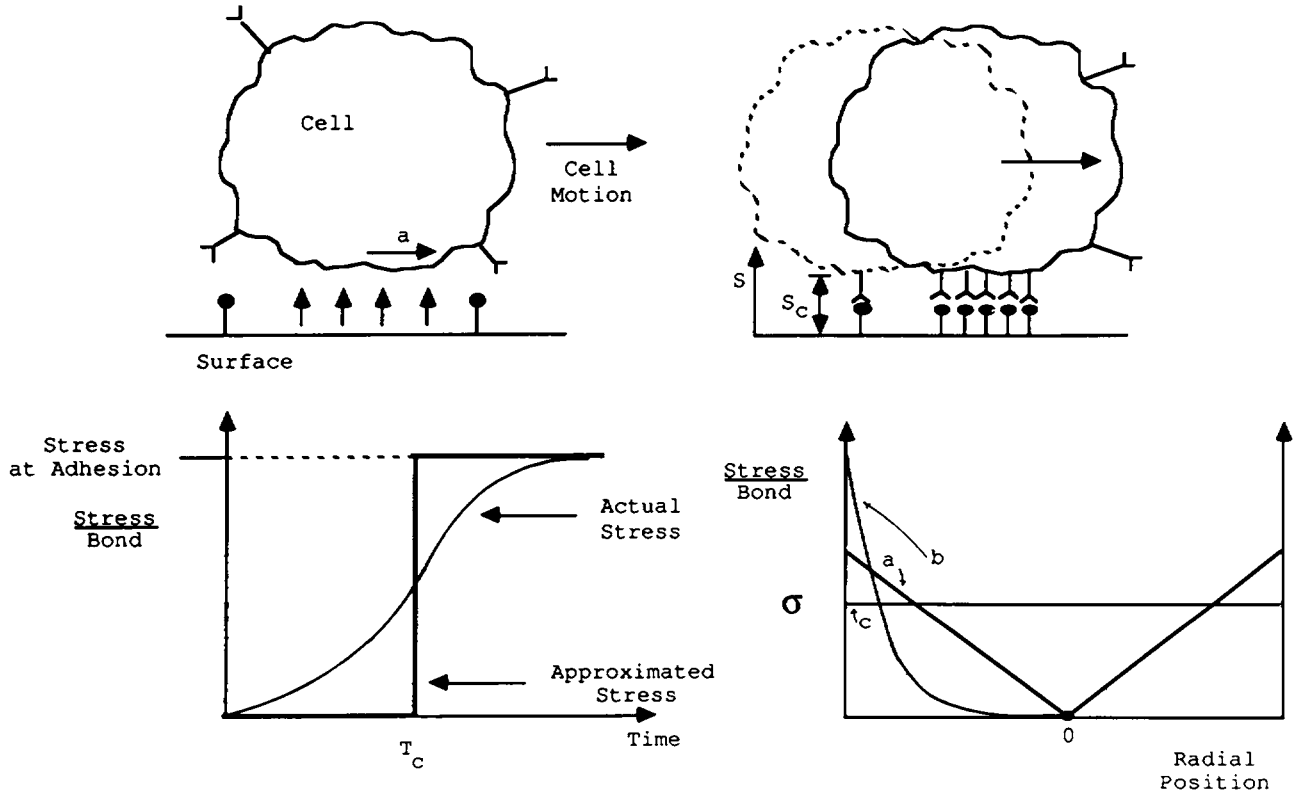

FIGURE 2 The basic assumptions of the present model are pictorially represented; these assumptions are described in the text. Hydrodynamic pressure causes flattening of the cell upon close approach, forming an area of radius a. During the contact time, the cell rolls forward to distribute its bonds in the contact area. Graphically, we show the idealized bond stress as a function of time and position in the contact area, and how they compare with their more exact counterparts. The radial stress distributions are due to (*a*) Schmid-Schonbein et al. (19), (*b*) Evans (20, 21) and (*c*) this paper.

opposes the external torque on the cell. The contact time is thus the time to which bonds have been distributed to the back edge of the contact area by the forward motion of the cell.

Our third assumption is that we can approximate the normal stress distribution such that the bonds are equally stressed in the contact area. Schmid–Schonbein (19) and Evans (20, 21) have pointed out that the normal stress distribution is most likely a function of position. Our assumed stress distribution compares with theirs as shown in Fig. 2. The most important factor regarding the stress distribution is how the normal stresses counter the applied torque to the cell; thus, it is not only the stress itself but the stress and the position within the contact area that are important. Therefore, stressed bonds near the center of the contact area have little effect on countering the torque.

By making these quite reasonable assumptions, we obtain a tractable set of ordinary differential equations in which the free and bound receptor densities depend only on time and not on position within the contact area. A balance on bond density, N_b, and free receptor density, N_a, within the contact area gives

$$\frac{dN_b}{dt} = k_f N_{l_0} N_a - k_r N_b \tag{1}$$

$$\frac{dN_a}{dt} = -k_f N_{l_0} N_a + k_r N_b + \Delta(N_{c_0} - N_a), \tag{2}$$

where Δ (1/time) is a coefficient that accounts for the accumulation of free receptors into the contact area, and N_{c_0} is the initial receptor density on the cell. The initial conditions, at $t = 0$, are

$$N_b = 0 \tag{3}$$

and

$$N_a = \frac{R_T}{4\pi R_c^2}, \tag{4}$$

where R_c is the cell radius.

The reverse rate constant, k_r, and the mass transfer rate, Δ, from Eqs. 1 and 2 have different forms when the bonds are unstressed ($t \le T_c$) or stressed ($t > T_c$). The reverse rate constant, k_r, takes its base value, k_r^0, when the bonds are unstressed; when the bonds are stressed, their lifetime is decreased. This is a concept we borrow from Bell (14), who first used it for receptor–ligand interactions, and was originally developed by Zhurkov (22) in his analysis of the kinetic fracture of solids. If F_t is the total force acting on the bonds, then the force per bond, F_b, is given by

$$F_b = \frac{F_t}{\pi a^2 N_b}. \tag{5}$$

Under stress, the reverse rate constant then becomes

$$k_r = k_r^0 \exp\left(\frac{\gamma F_b}{k_b T}\right). \tag{6}$$

Here, γ is the characteristic structural length for a solid bond, k_b is the Boltzmann constant, and T is the absolute temperature.

To calculate the force in Eq. 6, we assume that an adherent cell is in mechanical equilibrium with its surroundings. Therefore, the bonds counter the force and torque the passing fluid applies to the cell. The details of this analysis are found in Appendix I. The result is

$$F_t = 6\pi\mu R_c^2 SR \cdot \sqrt{\left(1 + \frac{S}{R_c}\right)^2 F^{s^2}\left(1 + \frac{9\pi^2 R_c^2}{16a^2}\right) + \left(1 + \frac{S}{R_c}\right) F^s \tau^s \frac{3\pi^{2s^2}_c}{4a^2} + \frac{(\pi R_c)^2}{32a^2}\tau^{s^2}}, \tag{7}$$

in which the force depends on the contact area size, and SR is the shear rate.

The transport rate constant, Δ, is (23),

$$\Delta = \frac{2D}{a^2} + \frac{2\Omega R_c}{\pi a}, \tag{8}$$

where Ω is the angular velocity of the cell, and where $\Omega = 0$ when the bonds are stressed and the cell is not rotating.

To estimate T_c, we assume the cell can move under the fluid stresses applied to it even when some bonds are present, depending on the position of those bonds in the contact area. The period of unstressed bond formation T_c is the sum of two components: the time from which the cell first comes in contact with the surface to which the first bond forms, and the time from the formation of the first bond to the time the bonds become stressed. The mean time to form a first bond is given by the solution of Eqs. 1 and 2 with no net accumulation of receptors, that is $\Delta = 0$, from $N_b = 0$ to $N_b = 1/\pi a^2$. This time is

$$T_1 = \frac{1}{k_f N_{l_0}} \ln\left(1 - \frac{1}{A_c N_{c_0}}\right)^{-1}. \tag{9}$$

The bonds will be fully stressed when they are well distributed over the contact area. If we think of the bonds being formed roughly in the center of this area during unstressed bond formation, then the mean time before the first bond reaches the edge is given by

$$T_2 = \frac{a}{V} \tag{10}$$

and

$$T_c = T_1 + T_2. \tag{11}$$

There is some question as to whether this initial formation is truly unstressed, since integral membrane proteins are sometimes attached to the cytoskeleton. For proteins in the plane of the membrane, however, it is generally true that a significant fraction is mobile (24, 25). Thus the only stress on a bond would be a drag force as it moves through the membrane, which should be negligible.

The contact area depends on the sum of normal forces acting on the cell, including forces of deposition such as gravity or hydrodynamic forces, nonspecific forces including van der Waals, electrostatic, and steric stabilization forces, and forces required to deform the cell. The force of deformation is that force required to deform the particle away from its unstressed shape, and it depends on cell mechanical properties. For example, it has been established that a red blood cell's membrane deformation can be described through knowledge of membrane shear and bending moduli (26–29). However, characterization of membrane deformation is insufficient to describe cell shapes in other cell types like leukocytes. Three-dimensional constitutive relations have been proposed to describe the deformation of these cells, and they appear to successfully explain their response to micropipet aspiration experiments (30, 31). So the precise relationship between external force and shape will vary with different cell types.

In general, the contact area will depend on a balance of forces:

$$0 = F_{\text{depositional}} + F_{\text{nonspecific}}(S, A_c) + F_{\text{deformation}}(S, A_c), \quad (12)$$

in which A_c is the contact area and S is the separation distance. We intend to calculate how adhesiveness varies with changes in the contact area. Although the precise relationship between external forces and contact area will remain to be elucidated, the effect of variations in nonspecific phenomena, such as greater van der Waals attraction or attenuated electrostatic repulsion, can be examined implicitly through contact area changes.

To summarize, we intend to solve the system of Eqs. 1 and 2 with initial conditions 3 and 4 in two time regimes: $t \le T_c$ (unstressed bonds) and $t > T_c$ (stressed bonds). The contact time T_c is related to fluid dynamical properties through the translational velocity. The differences in parameter values from unstressed to stressed bond formation are given by the differences between k_r and Δ in the two regimes:

$$\Delta = \begin{cases} \dfrac{2D}{a^2} + \dfrac{2\Omega R_c}{\pi a} & t \le T_c \\ \dfrac{2D}{a^2} & t > T_c \end{cases} \quad (13)$$

and

$$k_r = \begin{cases} k_r^0 & t \le T_c \\ k_r^0 \exp\left(\dfrac{\gamma F_b}{k_b T}\right) & t > T_c. \end{cases} \quad (14)$$

MODEL ANALYSIS

If we define the following dimensionless parameters

$$\tau = \frac{t}{T_c} \quad \eta_a = \frac{N_a}{N_{c_0}} \quad \eta_b = \frac{N_b}{N_{c_0}} \quad \theta = k_f N_{L_0} T_c$$
$$\beta = \frac{1}{4}\left(\frac{a}{R_c}\right)^2 \quad \kappa = \frac{k_r^0}{k_f N_{L_0}} \quad \alpha = \frac{\gamma F_t}{k_b T} \quad \delta = \frac{\Delta}{k_f N_{L_0}}, \quad (15)$$

the model equations become

$$\frac{d\eta_b}{d\tau} = \theta\left[\eta_a - \kappa\eta_b \exp\left(\frac{\alpha}{\beta R_T \eta_b}\right)\right] \quad (16)$$

$$\frac{d\eta_a}{d\tau} = \theta\left[-\eta_a + \kappa\eta_b \exp\left(\frac{\alpha}{\beta R_T \eta_b}\right) + \delta(1 - \eta_b)\right] \quad (17)$$

with initial conditions

$$\tau = 0 \; \eta_a = 1 \; \eta_b = 0, \quad (18)$$

TABLE 1
PARAMETER ESTIMATES

Parameter	Definition	Range	Reference
R_t	Receptor number	10^3–10^7	Bell (15), Capo et al. (42), Zigmond et al. (43), Klausner et al. (44), Mellman and Plutner (45)
D	Diffusivity	10^{-9}–10^{-12} cm^2/s	Axelrod et al. (24), Jacobson et al. (25)
A_c	Contact area	10^{-2}–5 μm^2	Bell (15), Capo et al. (42), Bell et al. (46)
γ	Bond interaction length	5×10^{-8} cm	Bell (15)
N_{L_0}	Ligand density	10^{10}–10^{13} molecules/cm^2	Rutishauser and Sachs (38)
k_{+1}	Forward intrinsic reaction rate	10^6–10^9 s^{-1}	Pecht and Lancet (33), Bell (15)
ΔH	Enthapy of reaction	−15.0–0.0 kcal/mol	Pecht and Lancet (33)
ΔS	Entropy of reaction	-4×10^{-2}–0 kcal/mol-K	Pecht and Lancet (33)
$\Delta H^{\ddagger}$	Enthalpy of activation	0.0–21.0 kcal/mol	Pecht and Lancet (33)
$\Delta S^{\ddagger}$	Entropy of activation	-10^2–0 kcal/mol-K	Pecht and Lancet (33)
R_{ab}	Radius of receptor–ligand interaction complex	5–10 Å	Pecht and Lancet (33), Bell (15)
T	Temperature	273–310 K	—

and where the difference in parameters from stressed to unstressed bond formation are denoted

$$\delta = \begin{cases} \dfrac{1}{k_f N_{l_0}} \left(\dfrac{2D}{a^2} + \dfrac{2\Omega R_c}{\pi a} \right) & \tau \le 1 \\ \dfrac{2D}{k_f N_{l_0} a^2} & \tau > 1 \end{cases} \tag{19}$$

and

$$\alpha = \begin{cases} 0 & \tau \le 1 \\ \dfrac{\gamma F_t}{k_b T} & \tau > 1. \end{cases} \tag{20}$$

We have solved this system of equations using standard phase-plane techniques (23, 32).

The parameters of Eq. 16 have significant physical meaning. The parameter θ is the product of the overall forward reaction rate and the contact time, and hence is the dimensionless bond formation rate. κ is the dimensionless dissociation constant, or inverse affinity. The parameter α is the energy that the bonds must withstand, scaled to the thermal energy. β is the dimensionless contact area and δ is the rate of transport of free receptors scaled to the forward reaction rate. For each combination of the parameters cited above, there will be a critical value of the dimensionless bond formation rate, namely $\theta_c = \theta_c(\kappa, \alpha, \beta, \tau_c, \delta)$ such that if $\theta \ge \theta_c$, adhesion will occur. This relationship can be used implicitly to determine the critical value of any parameter that will provide for adhesion given that the others are fixed. Thus, a wide range of parameter effects can be elucidated.

TABLE II
RECEPTOR-LIGAND BINDING AFFINITIES

Estimated $\frac{k_f}{k_r^0}$	Receptor–ligand system	Reference
cm²/molecules		
3.3×10^{-5}	Fc receptor/Fc-IgE	Pruzansky and Patterson (47)
8.8×10^{-7}	Chemotactic peptide receptor/ FNLLP peptide	Zigmond et al. (43)
8.8×10^{-6}	Transferrin receptor/diferric transferrin	Klausner et al. (44)
3.5×10^{-7}	Transferrin receptor/ apotransferrin	Klausner et al. (44)
3.5×10^{-7}	Fc Receptor/Fc-IgG	Mellman and Plutner (45)
1.8×10^{-5}	EGF Receptor/EGF	Dunn and Hubbard (48)
10^{-12}–10^{-1}	Antibody/hapten	Pecht and Lancet (33)

EGF, epidermal growth factor; FNLLP, formyl-norleucine-leucine-phenylalanine.

TABLE III
ESTIMATES FOR DIMENSIONLESS PARAMETERS

Dimensionless parameter	Definition	Range
α	Bond breakage energy	0–1,000
β	Contact area	10^{-4}–10^{-2}
κ	Dissociation constant	10^{-8}–10^{2}
δ	Receptor accumulation rate	10^{-2}–10^{2}
θ	Bond formation rate	10^{-4}–10^{1}

In Tables I–III, we show ranges of parameter values from the literature, along with references, for both dimensional and dimensionless parameters. Where important, we will make reference to particularly interesting parameter regimes.

GENERAL RESULTS

The one-to-one correspondence between required receptor number and affinity at different values of the dimensionless bond formation rate is illustrated in Fig. 3. Both decreasing bond formation rate and decreasing affinity will lead to an increase in the number of receptors required for adhesion. There are two physically meaningful asymptotes at low and high values of κ. At low κ (high affinity) the number of receptors required is independent of κ and

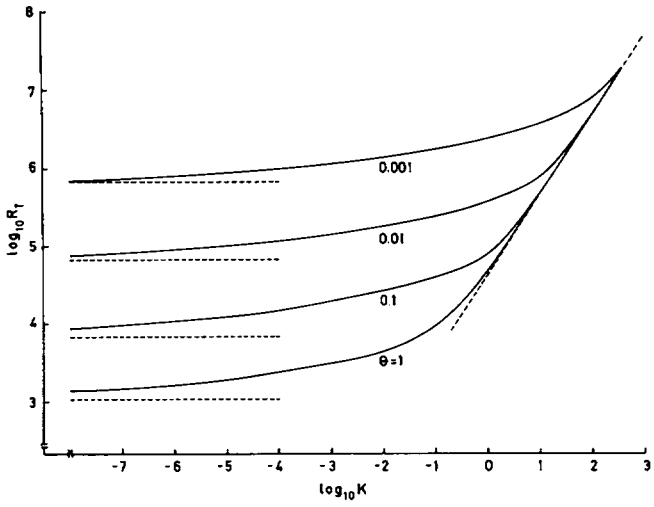

FIGURE 3 A plot of the number of receptors required for adhesion versus dimensionless dissociation constant at different bond formation rates indicates two expected trends: increasing bond formation rate means fewer receptors are required for adhesion at a fixed dimensionless dissociation constant, and an increasing dissociation constant means more receptors are required for adhesion at a fixed bond formation rate. Two sets of asymptotes are evident for high and low affinity. At high affinity, only one bond must be formed during the contact time for adhesion. At low affinity, the receptor number must be such that steady states are present in the phase plane. The two asymptotes have straightforward analytical forms as seen in the text. Here $\alpha = 25$, $D = 10^{-9}$ cm²/s, and $\beta = 1.5 \times 10^{-3}$.

depends only on the mean time necessary to form a single bond:

$$R_T = \frac{1}{\beta(1 - e^{-\theta})}. \quad (21)$$

This asymptote depends strongly on the bond formation rate and represents the "rate-controlled regime."

At high values of κ (low affinity) the number of receptors required is determined by an existence criterion for a stable steady solution to Eqs. 16 and 17. This asymptote is given by

$$R_T = \frac{\alpha\kappa e}{\beta}. \quad (22)$$

We can see that the required number of receptors is proportional to the inverse affinity, κ. This is the "affinity controlled" regime and represents an equilibrium controlled situation.

One of the variables under experimental control in an in vitro cell adhesion experiment is shear rate. In Fig. 4 we plot the permissible shear rate as a function of cell receptor number for several different affinities. Both higher receptor number and higher affinity allow for higher permissible shear rates. So, for example, a change in κ from 10 to 1 at a receptor number of 5×10^5 receptors can lead to a greater than threefold increase in the permissible shear rate from ~20 to over 60 s^{-1}. Therefore, a 10-fold decrease in the overall dissociation constant can lead to a significant increase in adhesiveness.

Previously, we argued that knowledge of the quantitative relationship between adhesion and contact area size provides useful information that ultimately may be tied to nonspecific forces and cell deformability. In Fig. 5, we show how the dimensionless maximum shear rate permitting adhesion (SR scaled to the overall forward reaction rate, $k_f N_{l_0}$) depends on the contact area for different affinities. For the highest affinities (lowest κ), an order of

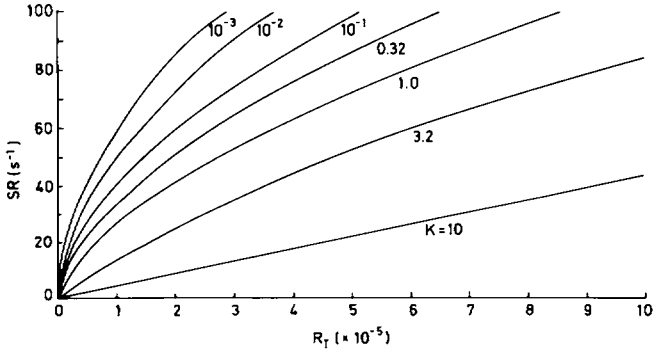

FIGURE 4 A plot of permissible shear rate versus receptor number at various values of the dimensionless dissociation constant shows that the permissible shear rate goes up as the dissociation constant goes down at constant receptor number or as the receptor number goes up at a fixed dissociation constant. $\beta = 3.183 \times 10^{-3}$, $D = 10^{-9}$ cm^2/s, and $k_f N_{l_0} = 10$ s^{-1}.

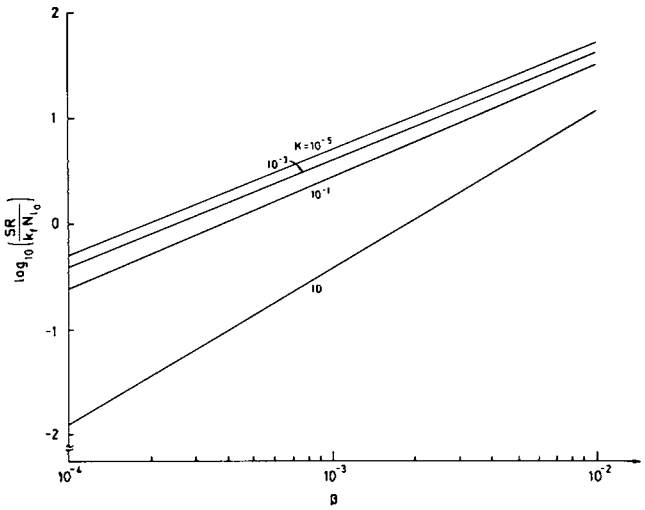

FIGURE 5 The strong dependence of the permissible dimensionless shear rate ($SR/k_f N_{l_0}$) for adhesion versus the dimensionless contact area, β, is represented on a log–log plot. The sensitivity of shear rate on contact area increases as the receptor–ligand affinity decreases. Here, $R_T = 5 \times 10^5$, $kN_{l_0}(6\pi\mu\gamma R_c^2)/k_b T = 0.5504$, and $D = 10^{-10}$ cm^2/s.

magnitude increase in contact area leads to an order of magnitude increase in the dimensionless permissible shear rate. Thus, permissive nonspecific interactions, which increase the size of the contact area, or less rigid cells, which show larger areas of contact under fixed external forces, should show great increases in adhesiveness. As the affinity decreases and we move toward the affinity controlled regime, the adhesiveness varies more sharply with contact area because of the sharp dependence of the bond breakage energy on contact area (as given by Eqs. 7 and 22).

It is not only the affinity between receptor and ligand but the rates of reaction that may control adhesion. This effect is enhanced in the rate-controlled regime. In Fig. 6, we plot the required number of receptors as a function of forward reaction rate $k_f N_{l_0}$ under a fixed external force. An increase in the overall forward reaction rate means an decrease in required receptor number; this effect is maximized in the rate-controlled regime (at high affinity) and is attenuated at low affinity.

Effects of Diffusivity and Temperature

We calculate the permissible shear rate for cells as the mobility of their receptors varies. We incorporate the effects of diffusivity on overall forward and reverse reaction rates as set forth by Bell (15). Fig. 7 shows that at high affinity (low κ), there is a dramatic increase in the permissible shear rate as the diffusivity is increased through a range of physically reasonable possibilities from 10^{-11} cm^2/s to 10^{-9} cm^2/s. This effect is only observed at high affinity since rate processes control there. Thus, there will be regimes in which diffusivity plays a crucial role in adhesion.

Temperature affects many different parameters. First,

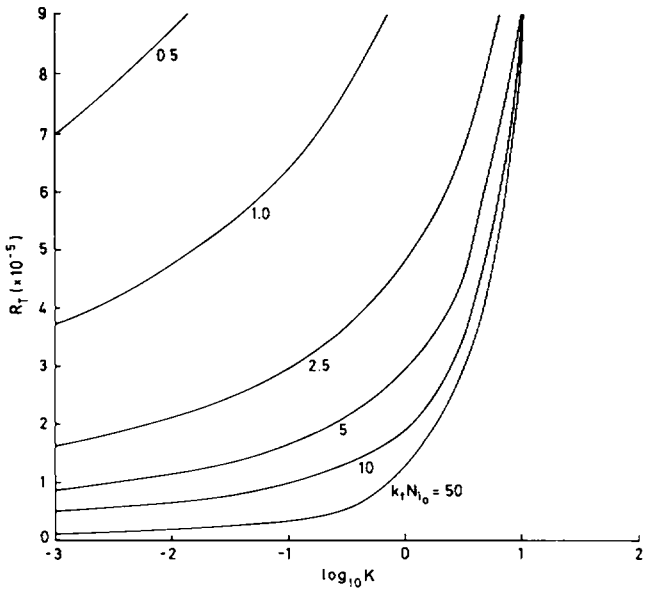

FIGURE 6 A plot of the required receptor number versus the dissociation constant at various overall forward reaction rates, $k_f N_{l_0}$, shows that not only does the affinity between ligand and receptor determine adhesiveness, but also the speed of reaction plays an important role. At any fixed dissociation constant an increase in $k_f N_{l_0}$ leads to a decrease in the number of receptors required for adhesion. At fixed $k_f N_{l_0}$, an increasing dissociation rate leads to an increase in the required number of receptors. $SR = 40\ s^{-1}$, $\beta = 3.183 \times 10^{-3}$, and $D = 10^{-9}\ cm^2/s$.

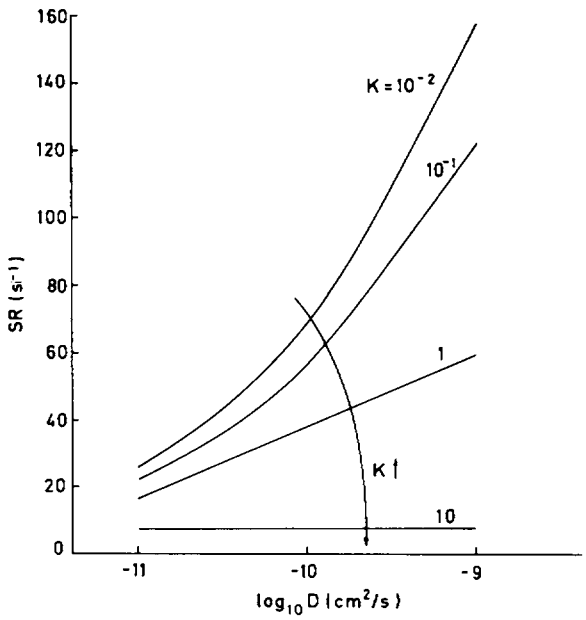

FIGURE 7 The permissible shear rate is plotted as a function of the receptor mobility in the plane of the membrane, D, at different values of the dimensionless dissociation constant, κ. The results show that the mobility is significantly important in determining adhesiveness when the dissociation constant is low (or the affinity is high) between receptor and ligand. However, when the dissociation constant is high (or the affinity is low) between receptor and ligand, adhesiveness is independent of receptor mobility. $R_T = 5 \times 10^5$, $\beta = 1.5 \times 10^{-3}$, and $k_{+1} = 5 \times 10^5$.

the bond breakage energy α decreases with increasing temperature because the viscosity of aqueous solutions decreases with increasing temperature, and because α is inversely proportional to temperature. Second, we expect the diffusional mobility to increase with increasing temperature (24, 25).

Lastly, both reaction rates and affinities are functions of temperature. Bell (15) has described how the overall forward reaction rate, k_f, depends on the forward intrinsic reaction rate, k_{+1}, and how the dimensionless affinity, κ, depends on the ratio of intrinsic reaction rates, k_{+1}/k_{-1}, for membrane bound reactants. Pecht and Lancet (33) have characterized antibody–hapten reactions according to the relationships

$$\frac{k_{+1}}{k_{-1}} = e^{-\Delta G/RT} \quad \Delta G = \Delta H - T\Delta S \tag{23}$$

and

$$k_{+1} = \frac{k_b T}{h} e^{-\Delta G^{\ddagger}/RT} \quad \Delta G^{\ddagger} = \Delta H^{\ddagger} - T\Delta S^{\ddagger}, \tag{24}$$

where Eq. 26 is the thermodynamic relationship between the Gibbs free energy change and the intrinsic affinity, and Eq. 27 is the Eyring equation. In these equations, ΔH and ΔS are the enthalpy and entropy changes of reaction; $\Delta G^{\ddagger}$, $\Delta H^{\ddagger}$, and $\Delta S^{\ddagger}$ are the free energy, enthalpy, and entropy changes of activation, and h is Planck's constant.

Using reasonable values for $\Delta H^{\ddagger}$, $\Delta S^{\ddagger}$, ΔH, and ΔS, and the reported dependencies of viscosity and mobility on temperature, we calculate the dependence of adhesion on temperature. We note that because the typical values reported by Pecht and Lancet for $\Delta H^{\ddagger}$ and ΔH are such that $\Delta H^{\ddagger} > 0$ and $\Delta H < 0$ (exothermic), the opposing effects of increasing temperature is to make adhesion more likely through increasing k_{+1} and D and decreasing α, and to make adhesion less likely through a decrease in the affinity; so the overall effect depends on the relative importance of these variables. In Fig. 8 *A*, we plot the permissible shear rate as a function of temperature for different values of the entropy change of reaction between receptor and ligand, when the enthalpy change of reaction between receptor and ligand is fixed. As ΔS decreases, the affinity decreases, the system approaches the affinity-controlled regime, and adhesivity progressively decreases with increasing temperature, first exhibiting a maximum in temperature, and then decreasing monotonically with increasing temperature.

We are cautious about drawing firm conclusions about the effect of temperature on adhesion, since we have not included how temperature affects cell deformability. Hence, we offer the above as a possibile explanation for situations in which adhesivity decreases with increasing temperature (as we shall discuss below), and one which is valid in situations where deformability is a weak function of temperature.

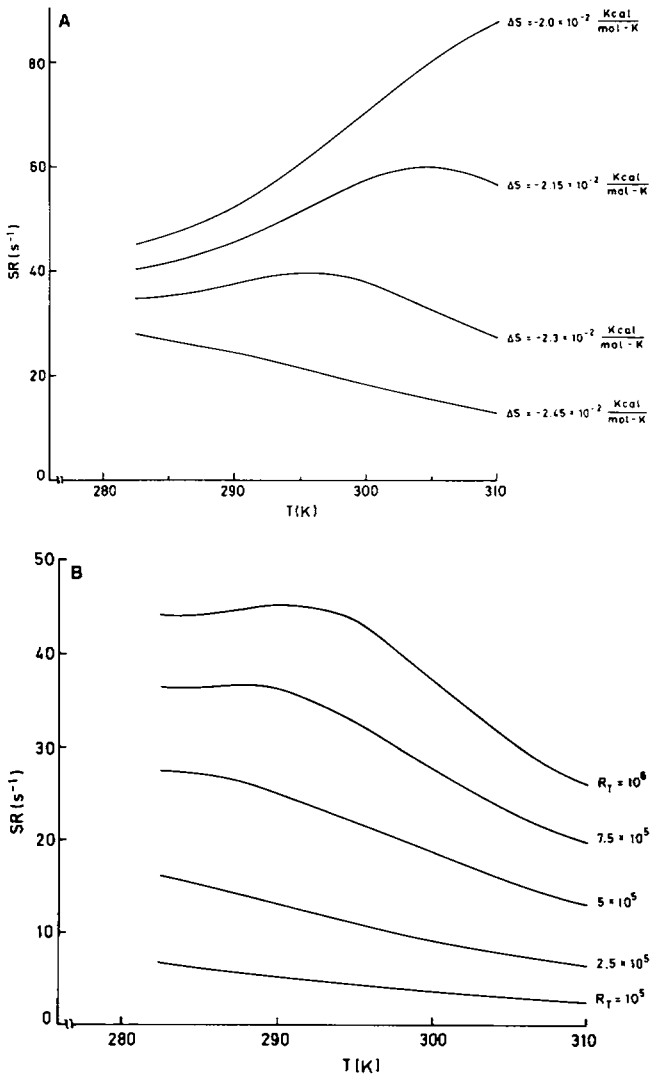

FIGURE 8 We investigate how adhesiveness depends on temperature in two hypothetical scenarios that might account for the differential adhesiveness of cell subpopulations. (*A*) The permissible shear rate is plotted as a function of temperature (K) for different values of the entropy change of reaction when the enthalpy change of reaction is constant. $R_T = 5 \times 10^5$, $\Delta H = -11.0$ kcal/mol, and $\beta = 3 \times 10^{-3}$. (*B*) The permissible shear rate is considered as a function of temperature for the case in which a cell has the same affinity of interaction between receptor and ligand, but different receptor number. The middle curve in *B* corresponds to the bottom curve in *A*. $\Delta H = -11.0$ kcal/mol, $\Delta S = -2.45 \times 10^{-2}$ kcal/mol-K, and $\beta = 3 \times 10^{-3}$. In *A* and *B*, the temperature dependence of viscosity is that of water, the temperature dependence of diffusivity is that reported by Jacobson (25), $N_{l_0} = 10^{10}$ molecules/cm², $\Delta H^{\ddagger} = 5.0$ kcal/mol, and $\Delta S^{\ddagger} = -7.0 \times 10^{-3}$ kcal/mol-K.

Testability

We have shown that for both high- and low-affinity interactions, analytical expressions can be found that relate the number of receptors required for adhesion on various other parameters. Here, we manipulate those analytical relationships to anticipate laboratory scenarios in which they might be tested. Two variables that are typically under an experimentalist's control are the shear rate, SR, and the ligand density, N_{l_0}. Thus we would like to know how adhesion depends quantitatively on those variables in the two different affinity regimes.

At high affinity the required receptor number is given in Eq. 21. In this regime, a cell will eventually adhere unless there are so few receptors in the contact area that a bond can never form. At high affinity, the distance travelled before adhesion, L_{AD}, is given (using relationships in Appendix I)

$$L_{AD} = R_c \ln\left[1 - \frac{1}{\beta R_T}\right]^{-1} \cdot \left(\frac{SR}{k_f N_{l_0}}\right)\left[\frac{\frac{1}{2}F^t\tau^s - \left(1 + \frac{S}{R_c}\right)F^s\tau^r}{F^t\tau^r - F^r\tau^t}\right]. \quad (25)$$

Note the distance travelled before adhesion depends linearly on SR and inversely on N_{l_0}. In Table IV, we have given values of the bracketed function on the right-hand side of Eq. 25 from values given by Goldman et al. (34, 35) for different values of the separation distance. To further facilitate the interpretation, Fig. 9 *A* shows the dependence of L_{AD}/R_c on $SR/k_f N_{l_0}$ for different values of βR_T. This linear relationship should be seen experimentally.

At low affinity, the appropriate asymptotic relationship (Eq. 22) may be manipulated to give (after substitution from Appendix I)

$$\frac{6\pi\mu\gamma R_c^2 SR}{k_b T} = \frac{\beta^{3/2} R_T}{e}\left(\frac{k_f N_{l_0}}{k_r^0}\right) \cdot \frac{1}{\sqrt{\left(1 + \frac{S}{R_c}\right)^2 F^{s^2}\left(\frac{9\pi^2}{64} + \beta\right) + \frac{3\pi^2}{16}F^s\tau^s\left(1 + \frac{S}{R_c}\right) + \frac{\pi^2}{144}\tau^{s^2}}}. \quad (26)$$

The permissible shear rate is proportional to the ligand density at low affinity. As before, we have tabulated the quantity on the right-hand side of Eq. 26 and have given it as a function of several values of β in Table V. We have also plotted this relationship in Fig. 9 *B*. The physical trends seen in the high-affinity regime are drastically

TABLE IV
VALUES FOR FUNCTION IN EQ. 25

$\frac{S}{R_c}$	$\frac{\frac{1}{2}F^t\tau^s - \left(1 + \frac{S}{R_c}\right)F^s\tau^r}{F^t\tau^r - F^r\tau^t}$
2×10^{-3}	0.4293
3×10^{-3}	0.4507
4×10^{-3}	0.4660
5×10^{-3}	0.4809
7.5×10^{-3}	0.5186
10^{-2}	0.5564

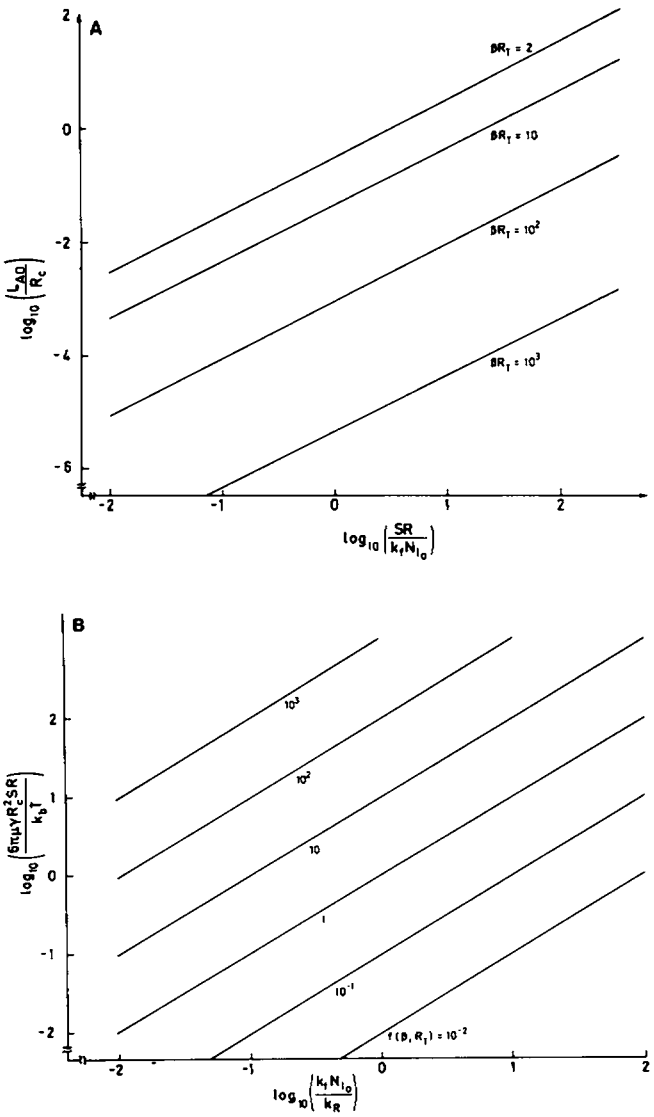

FIGURE 9 The analytical testable relationships (Eqs. 29 and 31) are represented graphically for high-affinity (A) and low-affinity (B) regimes. A gives the length travelled before adhesion as a function of shear rate or ligand density, appropriate at high affinity. B gives the relationship at low affinity for the dependence of permissible shear rate on ligand density. Here, $S/R_c = 3 \times 10^{-3}$. Also, $f(\beta, R_t)$ represents the product of all terms on the right-hand side of Eq. 26 other than $k_f N_{l_0}/k_r$.

different than those seen in the low-affinity regime. These results suggest that by varying shear rate or ligand densities, conclusions can be made about the affinity of receptor–ligand interaction when affinity data do not exist.

It should be noted that the values of the dissociation constant, κ, at which the asymptotic solutions given by Eqs. 21 and 22 accurately approximate the exact solution depend on the bond breakage energy. For both asymptotes, matching is more accurate at progressively lower values of κ for greater values of α (greater shear rates). Therefore, at low values of κ, departure from asymptotic values will be seen at higher shear rates (~100 s^{-1}). However, the asymptotes remain rough guides for behavior in the two regimes.

TABLE V
VALUES FOR FUNCTION IN EQ. 26

$\frac{S}{R_c}$	$\sqrt{\left(1+\frac{S}{R_c}\right)^2 F^{*2}\left(\frac{9\pi^2}{64}+\beta\right)+\frac{3\pi^2}{16}F^{*}\tau^{*}\left(1+\frac{S}{R_c}\right)+\frac{\pi^2}{144}\tau^{*2}}$	
	$\beta = 2.5 \times 10^{-4}$	$\beta = 5 \times 10^{-3}$
2×10^{-3}	2.6569	2.6595
3×10^{-3}	2.6581	2.6607
4×10^{-3}	2.6594	2.6623
5×10^{-3}	2.6606	2.6632
7.5×10^{-3}	2.6637	2.6662
10^{-2}	2.6667	2.6693

Comparison with Experiment

At the present time it is difficult to compare our theory with any particular data in the existing literature. The various quantities involved in this paper have not been determined in a single experiment on one particular system. However, almost all of these quantities have been determined individually for a variety of systems. Experiments performed in a parallel plate flow chamber assay (7) with neutrophil leukocytes adhering to antibody-coated glass indicate that adhesion occurs at a shear rate of ~40 s^{-1}, which is within the range of shear rates this paper predicts to be relevant.

Recently, Mege et al. (36) reported experiments for the adhesion of P388D1 mouse macrophage-like lines to glass capillaries in well developed viscous flow. They reported permissible shear rates between 10 and 115 s^{-1} and claimed the critical step necessary for adhesion was first bond formation. They also reported that the formation of such a bond took 30 s, and that the length a cell travelled before adhesion depended on shear rate. The value of 30 s

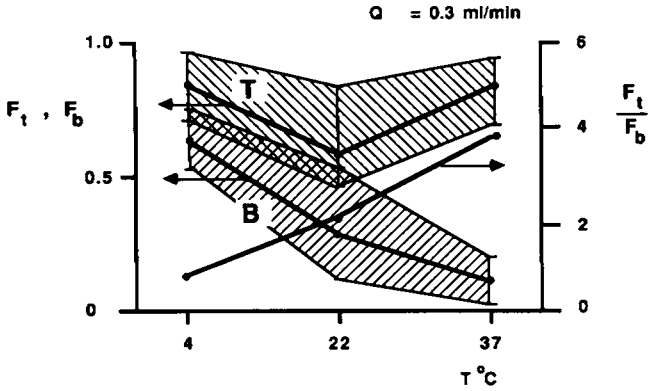

FIGURE 10 Data for the retention of T and B lymphocyte populations on an SBA-coated cell affinity column taken from Hertz (37). The fraction of cells of each type retained, F, is given as a function of temperature at a fixed flow rate, Q = 0.3 ml/min. The data show that there is a weak temperature dependence on T cell retention, but a strong reduction in B cell retention as the temperature increases. The center line represents the mean values and the shaded area represents the scatter in the data. The selectivity for retention, F_T/F_B, increases with increasing temperature.

seems rather long, and a possibility for its overestimation is the neglect of slower sedimentation velocities at small separation distances. Assuming the data correct, and using a rough estimate of $\beta R_T \sim 10$, we calculate that 30 s to form the first bond means $k_f N_{l_0} = 10^{-3}$. If k_f is at 1% of its diffusion limit, $\sim 6 \times 10^{-12}$ cm^2/s, the density of binding sites on the surface is 10^9 molecules/cm^2. Comparison of reported values of lengths travelled before adhesion (mean of four experiments) shows <0.1 cm at a shear rate of 14.3 s^{-1}, 0.13 cm at 28.7 s^{-1}, 0.27 cm at 57.4 cm^{-1}, and 2 cm at 115 s^{-1}. According to Eq. 25, the theoretically predicted length travelled before adhesion should double with shear rate. The experimentally measured length travelled before adhesion changes by factors of 1.26, 2.14, and 7.4 as the shear rate is doubled. So there is relatively good agreement between theory and experiment at low shear rates. The breakdown at high shear rates suggests the high-affinity asymptote cannot completely characterize adhesion.

In Fig. 10, we plot data from Hertz (37), for the fractional retention of both T and B lymphocytes on a soybean agglutinin (SBA) cell affinity column as a function of temperature at a fixed flow rate.

We note that the retention of the T lymphocyte population is a relatively weak function of temperature, while the retention of the B cell population decreases with increasing temperature. Using Fig. 8, we can offer hypotheses to explain the different response of these two cell types. To do this, we compare cell retention at fixed shear rate, say 20 s^{-1}, and note that the bottom most curve in Fig. 8 *A* indicates a B cell–like behavior: the adhesiveness decreases with increasing temperature. However, either an increase in the affinity at a fixed number of receptors (5×10^5) or a doubling in receptor number at fixed affinity ($\Delta S = -2.45 \times 10^{-3}$ kcal/mol-K; Fig. 8 *B*) would give T cell–like behavior: a population whose adhesiveness was not diminished between 9° and 37°C at 20 s^{-1}. This analysis also indicates the telling experiments that could be performed to distinguish further between the alternative hypotheses. A series of experiments performed at twice the flow rate (40 s^{-1}) would distinguish between cells at lower affinities ($\Delta S = -2.3 \times 10^{-2}$ kcal/mol-K), which would not bind at any temperature, higher affinities ($\Delta S = -2.0 \times 10^{-2}$ kcal/mol-K), which would bind at all temperatures, and higher receptor number ($R_t = 10^6$), which would exhibit adhesion at low but not high temperatures.

Rutishauser and Sachs (38) also reported a difference in temperature-dependent binding of L1210 murine lymphoma cells to lectin-coated fibers. In these experiments, ligand densities varied from 10^{10} to 10^{13} molecules/cm^2. The fibers are long cylinders that have diameters about twelve times that of the cells involved, so significant shear is occurring during cell–fiber contact. As temperature decreased from 22° to 0°C, adhesion greatly decreased on concanavalin A (conA)–coated fibers, but increased slightly on SBA-coated fibers. A tentative explanation might be that rate processes are crucial on conA fibers, and not on SBA fibers. Further, we compare our theory with their data on the lectin density dependence of binding to these two lectins to test our hypothesis that conA is a higher affinity ligand to these cells than is SBA. The data and comparison to theory are given in Table VI. We calculate permissible shear rates for receptor–ligand interactions of low affinity ($k_f/k_r = 10^{-11}$ cm^2) and high affinity ($k_f/k_r = 10^{-5}$ cm^2). In these calculations, $R_t = 5 \times 10^5$, $\beta = 3 \times 10^{-3}$, and we assume $k_f \sim 2\pi D$ (diffusion limit) for both ligands. The shear rates predicted are rather large, in accordance with the large velocities in the experiment (10 cm/s) (38). If 600 s^{-1} is a cutoff for substantial adhesion (>200 cells/cm), we predict 2.1×10^{12} and 2×10^{11} molecules/cm^2 for SBA and conA, respectively, to be the lowest permitted ligand densities, and this agrees with experiment. If ~300 s^{-1} is a cutoff for measurable adhesion, then 5×10^{11} and $\sim 10^{10}$ molecules/cm^2 for SBA and conA, respectively, would be nonpermissive. These are in rough quantitative agreement with experiment. Although we are simplifying the complex fluid forces in this experiment, the hypothesis that receptor–ligand affinity is different for these two ligands accounts for the temperature and ligand density effects in these two systems.

TABLE VI
COMPARISON OF MODEL TO EXPERIMENTAL RESULTS

Lectin site density	L1210 cells/cm fiber*		Calculated permissible shear rates	
	ConA coated	SBA coated	$\frac{k_f}{k_r} = 10^{-5}$	$\frac{k_f}{k_r} = 10^{-11}$
sites/cm^2			s^{-1}	
2.1×10^{10}	384	243	1,684	706
10^{12}	328	20	1,166	476
7×10^{11}	298	0	977	391
3.5×10^{11}	260	0	690	263
1.8×10^{11}	93	0	493	177
8.8×10^{10}	31	0	343	112

*Rutishauser and Sachs, 1975 (38).

As Bell (15) has pointed out, glutaraldehyde-fixed cells do not bind to the fibers in these experiments because receptor mobility is zero and $k_f \sim 0$. This is consistent with Fig. 6, which shows that a value of $k_f \sim 0$ means adhesion will not occur at any reasonable receptor number.

Thus, we have shown how the analysis can be used to explain a wide variety of adhesive phenomena, how it provides a simple explanation for seemingly conflicting experimental observations of the effect of temperature on adhesion, and how it can be used to suggest telling experiments that will further test hypotheses.

DISCUSSION

This paper presents a theoretical description of the receptor-mediated adhesion of cells to surfaces, and the distractive fluid flow acts principally tangent to the surface. Our analysis allows us to predict when a cell will adhere on the basis of fluid mechanical forces acting on the cell, the density of ligand molecules, the number of cell surface receptors, the speed at which receptors bind with ligand, the affinity of receptors for ligand, and the mobility of receptors in the plane of the membrane.

We make an effort to show how variables that are often under an experimentalist's control, like ligand density, temperature, or shear rate, would affect adhesiveness, thus providing testable relationships for future experiments. Also, we use our model to explain a variety of observed phenomena.

We find two distinct regimes in which adhesiveness is controlled by different mechanisms. In the "rate-controlled regime," the rate of reaction dominates over other effects in determining whether adhesion will occur. In the "affinity-controlled" regime, the affinity dominates over other processes. Knowledge of these two regimes allows us to understand the complex effects of receptor diffusivity and temperature on adhesion. At very high or very low affinity, these two regimes present themselves in simple analytical forms, enhancing the predictability and testability of the model.

The range of permissible shear rates we predict include shear rates (~10–50 s^{-1}), which are found in in vitro experiments, such as the parallel plate flow chamber assay (5, 6) and cell affinity chromatography (9), as well as those (~100–500 s^{-1}) found in the post capillary venules (19, 39, 40). However, a complete description of adhesion in these vessels must incorporate cell–cell interactions and inertial effects (41), and is therefore beyond the scope of this paper. In general, the methods of this paper can be extended to include cell deformability, surface structures specific for adhesionlike microvilli, stochastic binding, population heterogeneity, and spatially dependent stress distributions within the contact area. Such analyses, along with reproducible experiments designed for the quantitative study of cell adhesion, will aid in the understanding of adhesion and therefore provide for a more complete understanding of biological processes that involve it.

APPENDIX I

To calculate the forces on the bonds, we assume the forces and the torques exerted by the bonds must place the particle in mechanical equilibrium (see Fig. A1). The bonds in the contact area act both parallel to the direction of flow and normal to the cell surface. The action of the bonds in the contact area tangent to be surface balances the translational force due to shear; however, this pulling force imparts a torque on the cell. Thus, there are two additive torques that the bonds must resist: that due to the passing fluid and the other due to the bonding force. If the bonds are to resist the motion of the cell, they must impart forces on the cell that are equal and opposite to the stresses the cell applies to the bonds. The effect each bond has on diminishing the torque on the cell depends on the distance the bond is from the projection of the center of mass normal to the surface. Bonds very close to this projected point are less able to resist the torque because of their short lever arm.

The equations of mechanical equilibrium of the cell become (*a*) Force balance in the *x*-direction:

$$0 = F_s + F_b^x. \tag{A1}$$

(*b*) Torque balance in the *z*-direction:

$$0 = \tau_s + F_b^x R_c + \int_0^{2\pi} \int_0^a \sigma N_b |r \cos\theta| r \, dr \, d\theta, \tag{A2}$$

where subscripts s and b denote that due to shear and bonding, respectively; σ is the force exerted per bond; and θ and r are the angular and radial coordinates of the contact area. If the force per bond and bond densities are constant over the contact area, and if we integrate the expression in Eq. 12, the resulting bond requirements become: (*a*) Force balance *x*-direction:

$$F_b^x = -F_s. \tag{A3}$$

(*b*) Torque balance *z*-direction:

$$F_b^y = -\frac{3\pi}{4a}(\tau_s + F_b^x R_c). \tag{A4}$$

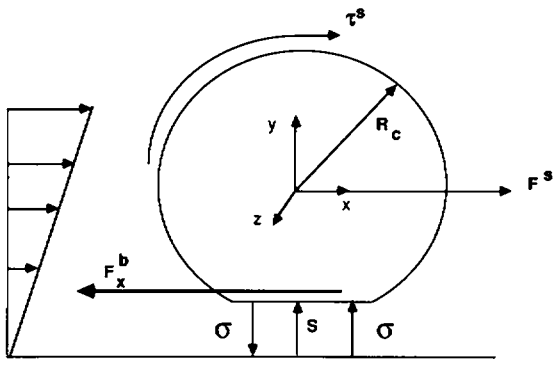

FIGURE A1 An adherent cell is assumed to be in mechanical equilibrium, and therefore has no net force acting on and no net torque acting around its center of mass. The shear force in the *x* direction imparted on the cell by the passing fluid, F^s, is the balanced by a bonding force, denoted F_x^b, equal in magnitude to F^s and acting in the opposite direction. This bonding force imparts a torque of magnitude $F^s R_c$ on the cell in the *z* direction which, along with the torque imparted by the external fluid, τ^s, must be balanced by normal stresses acting in the contact area, characterized by σ, the force per bond.

The total force, required by all the bonds, is given by

$$F_t = \sqrt{(F_b^x)^2 + (F_b^y)^2}. \tag{A5}$$

In a viscous shear field, the forces and torques on the cell due to the passing fluid, given by Goldman et al. (34, 35), are

$$F_s = 6\pi\mu R_c^2\left(1 + \frac{S}{R_c}\right) SR\, F^s\left(\frac{S}{R_c}\right) \tag{A6}$$

and

$$\tau_s = 4\pi\mu R_c^3\, SR\, \tau^s\left(\frac{S}{R_c}\right), \tag{A7}$$

in which F^s and τ^s are functions of dimensionless separation distance only, and SR is the fluid shear rate defined by

$$SR = \left(\frac{\partial v_f(s)}{\partial s}\right)\Bigg|_{s=0}, \tag{A8}$$

with v_f as the fluid velocity. Therefore, the total force F_t is

$$F_t = 6\pi\mu R_c^2 SR \cdot \sqrt{\left(1 + \frac{S}{R_c}\right)^2 F^{s^2}\left(\frac{9\pi^2 R_c^2}{16a^2} + 1\right) + \frac{3\pi^2 R_c^2}{4a^2} F^s\tau^s\left(1 + \frac{S}{R_c}\right) + \frac{\pi^2 R_c^2}{32a^2}\tau^{s^2}} \tag{A9}$$

which is Eq. 7 of the text. We should note that our presupposition about the way the bonds act means that the bonds impart no net force on the cell normal to the cell surface.

The solution of Goldman et al. also gives the translational and angular velocities when the cell is unstressed. For a cell that has a small density difference ($\Delta\rho$ = 0.05 g/cm^3) with respect to the fluid, the translational and angular velocities, V and Ω, are given

$$V = SR \cdot R_c \frac{\frac{1}{2}F^t\tau_s - \left(1 + \frac{S}{R_c}\right)F^s\tau^r}{F^t\tau^r - F^r\tau^t} \tag{A10}$$

$$\Omega = SR \frac{\left(1 + \frac{S}{R_c}\right)\tau^t F^s - \frac{1}{2}F^t\tau_s}{F^t\tau^r - F^r\tau^t}, \tag{A11}$$

in which F denotes force, τ denotes torque, the superscripts s, r, and t denote shear, rotation, and translation, and all of these are dimensionless quantities that are functions of separation distance only as defined by Goldman et al. Through these expressions, the dependence of dimensionless quantities that are functions of velocity can be written as a function of SR.

The authors thank Ms. Jennifer Linderman for providing rate constant data from the literature for various receptor–ligand systems.

This work has been supported by a National Science Foundation Presidential Young Investigator Award to D. A. Lauffenburger, along with a grant from E. I. DuPont de Nemours and Co., Inc.

Received for publication 5 January 1987 and in final form 19 May 1987.

REFERENCES

1. Morat, H. Z. 1985. The Inflammatory Reaction. Elsevier Science Publishers, Amsterdam.
2. Nicolson, G. L. 1982. Cancer metastasis: organ colonization and the cell-surface properties of malignant cells. *Biochim. Biophys. Acta.* 695:113–176.
3. Chin, Y.-H., R. Rasmussen, A. G. Cakiroglu, and J. J. Woodruff. 1984. Lymphocyte recognition of lymph node high endothelium. VI. Evidence of distinct structures mediating binding to high endothelial cells of lymph nodes and Peyer's patches. *J. Immunol.* 133:2961–2965.
4. Butcher, E., R. Scollay, and I. Weissman. 1980. Organ specificity of lymphocyte migration: mediation by highly selective lymphocyte interaction with organ specific determinants on high endothelial venules. *Eur. J. Immunol.* 10:556–561.
5. Doroszewski, J. 1980. Short-term and incomplete cell-substrate adhesion. *In* Cell Adhesion and Motility. A. S. G. Curtis and J. D. Pitts, editors. Cambridge University Press, Cambridge, UK. 171–197.
6. Forrester, J. V., and J. M. Lackie. 1984. Adhesion of neutrophils under conditions of flow. *J. Cell Sci.* 70:93–110.
7. Wilkinson, P. C., J. M. Lackie, J. V. Forrester, and G. A. Dunn. 1984. Chemokinetic accumulation of human neutrophils on immune complex coated substrata: analysis at a boundary. *J. Cell Biol.* 99:1761–1768.
8. Wigzell, H., and B. Andersson. 1969. Cell separation on antigen-coated columns: elimination of high rate antibody forming cells and immunological memory cells. *J. Exp. Med.* 129:23–36.
9. Hertz, C. M., D. J. Graves, D. A. Lauffenburger, and F. T. Serota. 1985. Use of cell affinity chromatography for separation of lymphocyte subpopulations. *Biotech. Bioeng.* XXVII:603–612.
10. Juckett, D. A., and D. E. Hultquist. 1983. Chromatography of erythroblasts on immobilized transferrin. *Proc. Soc. Exp. Biol. Med.* 172:79–83.
11. Kimura, A., H. Wigzell, G. Holmquist, B. Ersson, and P. Carlsson. 1979. Selective affinity fractionation of murine cytotoxic T lymphocytes (CTL): unique lectin specific binding of the CTL associated surface glycoprotein, T-145*. *J. Exp. Med.* 149:473–484.
12. Baran, M. V., D. M. Allen, S. R. Russell, M. E. Scheetz, II, and J. F. Monthony. 1982. Cell sorting using a universally applicable affinity chromatography matrix: solid-phase anti-fluorescein isothiocyanate antibody. *J. Immunol. Methods.* 53:321–334.
13. Sharma, S. K., and P. P. Mahendroo. 1980. Affinity chromatography of cells and cell membranes. *J. Chromatogr.* 184:471–499.
14. Bell, G. I. 1981. Estimate of the sticking probability for cells in a uniform shear flow with adhesion caused by specific bonds. *Cell. Biophys.* 3:289–304.
15. Bell, G. I. 1978. Models for the specific adhesion of cells to cells. *Science (Wash. DC).* 200:618–627.
16. Dimitrov, D. S., and I. B. Ivanov. 1978. Hydrodynamics of thin liquid films. On the rate of thinning of microscopic films with deformable interfaces. *J. Colloid Interface Sci.* 64:97–106.
17. Dimitrov, D. S. 1983. Dynamical interactions between approaching surfaces of biological interest. *Prog. Surf. Sci.* 14:295–424.
18. Dimitrov, D. S., N. Stoicheva, and D. Stefanova. 1984. A simple interpolation formula for the rate of approach of particles or cells with tension controlled shapes at arbitrary separations. *J. Colloid Interface Sci.* 98:269–271.
19. Schmid-Schonbein, G. W., Y.-C. Fung, and B. W. Zweifach. 1975. Vascular endothelium-leukocyte interactions: sticking shear force in venules. *Circ. Res.* 36:173–185.
20. Evans, E. A. 1985. Detailed mechanics of membrane-membrane adhesion and separation. I. Continuum of molecular crossbridges. *Biophys. J.* 48:175–183.
21. Evans, E. A. 1985. Detailed mechanics of membrane-membrane adhesion and separation. II. Discrete kinetically trapped cross-bridges. *Biophys. J.* 48:185–192.
22. Zhurkov, S. V. 1965. Kinetic concept of the fracture of solids. *Int. J. Fract. Mech.* 1:311–323.

23. Hammer, D. A. 1987. Ph.D. Thesis. University of Pennsylvania, Philadelphia, PA.
24. Axelrod, D., A. Wright, W. Webb, and A. Horowitz. 1978. Influence of membrane lipids on acetylcholine receptor and lipid probe diffusion in cultured myotube membrane. *Biochemistry*. 17:3604–3609.
25. Jacobson, K., D. O'Dell, and J. T. August. 1984. Lateral diffusion of a 80,000 dalton glycoprotein in the plasma membrane of murine fibroblasts: relationships to structure and function. *J. Cell Biol.* 99:1624–1633.
26. Evans, E. A., and R. Skalak. 1981. Mechanics and Thermodynamics of Biomembranes. CRC Press, Boca Raton, FL.
27. Evans, E. A. 1983. Bending elastic modulus of red blood cells membrane derived from the buckling instability in micropipet aspiration tests. *Biophys. J.* 43:27–30.
28. Fischer, T. M., C. W. M. Haest, M. Stohr-Liesen, H. Schmid-Schonbein, R. Skalak. 1981. The stress-free shape of the red blood cell membrane. *Biophys. J.* 34:409–422.
29. Zarda, P. R., S. Chien, and R. Skalak. 1977. Elastic deformations of red blood cells. *J. Biochem.* 10:211–221.
30. Schmid-Schonbein, G. W., K. P. Sung, H. Torzeren, R. Skalak, and S. Chien. 1981. Passive mechanical properties of human leukocytes. *Biophys. J.* 36:243–256.
31. Skalak, R., G. W. Schmid-Schonbein, and S. Chien. 1982. Analysis of white blood cell deformation. *In* White Blood Cells: Morphology and Rheology as Related to Function. U. Bagge, G. V. R. Born, and P. Gaehtgens, editors. 1–10.
32. Perlmutter, D. D. 1972. Stability of Chemical Reactors. Prentice-Hall, Inc., Englewood Cliffs, NJ. 71–126.
33. Pecht, I., and D. Lancet. 1977. Kinetics of antibody-hapten interactions. *Mol. Biol. Biochem. Biophys.* 24:306–337.
34. Goldman, A. J., R. G. Cox, and H. Brenner. 1967. Slow viscous motion of a sphere parallel to a plane wall: I. Motion through a quiescent fluid. *Chem. Eng. Sci.* 22:637–652.
35. Goldman, A. J., R. G. Cox, and H. Brenner. 1967. Slow viscous motion of a sphere parallel to a plane wall: II. Couette Flow. *Chem. Eng. Sci.* 22:653–659.
36. Mege, J. L., C. Capo, A. M. Benoliel, and P. Bongrand. 1986. Determination of binding strength and kinetics of binding initiation: a model study made on the adhesive properties of P388D1 macrophage-like cells. *Cell. Biophys.* 8:141–160.
37. Hertz, C. 1982. MS Thesis, University of Pennsylvania, Philadelphia, PA.
38. Rutishauser, U., and L. Sachs. 1975. Receptor-mobility and the binding of cells to lectin coated fibers. *J. Cell Biol.* 66:76–85.
39. Atherton, A., and G. V. R. Born. 1972. Quantitative investigations of the adhesiveness of circulating polymorphonuclear leukocytes to blood vessel walls. *J. Physiol. (Lond.).* 222:447–474.
40. Cooney, D. O. 1976. Biomedical Engineering Principles: An Introduction to Fluid, Heat, and Mass Transport Processes. Vol. 2. Marcel Dekker, Inc., New York.
41. Goldsmith, H. L., and S. Spain. 1984. Margination of leukocytes in blood flow through small tubes. *Microvasc. Res.* 27:204–222.
42. Capo, C., F. Garrouste, A.-M. Benoliel, P. Bongrand, A. Ryter, and G. I. Bell. 1982. Concanavalin-A-mediated thymocyte agglutination: a model for a quantitative study of cell adhesion. *J. Cell. Sci.* 56:21–48.
43. Zigmond, S. H., S. J. Sullivan, and D. A. Lauffenburger. 1982. Kinetic analysis of chemotactic peptide receptor modulation. *J. Cell Biol.* 92:34–43.
44. Klausner, R. D., G. Ashwell, J. van Rensoude, J. B. Harford, and K. R. Bridges. 1983. Binding of apo-transferrin to K562 cells: explanation of the transferrin cycle. *Proc. Natl. Acad. Sci. USA.* 80:2263–2266.
45. Mellman, I., and H. Plutner. 1964. Internalization and degradation of macrophage Fc receptors bound to polyvalent immune complexes. *J. Cell Biol.* 98:1170–1177.
46. Bell, G. I., M. Dembo, and P. Bongrand. 1984. Cell adhesion: competition between non-specific repulsion and specific binding. *Biophys. J.* 45:1051–1064.
47. Pruzansky, J. J., and R. Patterson. 1986. Binding constants of IgE on human blood basophils for IgE. *Immunology.* 58:257–262.
48. Dunn, W. A., and A. L. Hubbard. 1984. Receptor-mediated endocytosis of epidermal growth factory by hepatocytes in the perfused rat liver: ligand and receptor dynamics. *J. Cell Biol.* 98:2148–2159.